INTERFACE FOCUS

rsfs.royalsocietypublishing.org

Research

Cite this article: Roik NV, Belyakova LA. 2016 Mesoporous silica nanoparticles equipped with surface nanovalves for pH-controlled liberation of doxorubicin. *Interface Focus* **6**: 20160041. http://dx.doi.org/10.1098/rsfs.2016.0041

One contribution of 12 to a theme issue 'Multifunctional nanostructures for diagnosis and therapy of diseases'.

Subject Areas:
biomaterials, nanotechnology

Keywords:
aromatic amino group, β-cyclodextrin, nanovalve, doxorubicin, loading, release

Author for correspondence:
N. V. Roik
e-mail: roik_nadya@ukr.net

Mesoporous silica nanoparticles equipped with surface nanovalves for pH-controlled liberation of doxorubicin

N. V. Roik and L. A. Belyakova

Chuiko Institute of Surface Chemistry of NAS of Ukraine, 17 General Naumov Street, Kyiv 03164, Ukraine

NVR, 0000-0001-6286-8583

Silica carriers equipped with molecular and supramolecular pH-sensitive nanovalves were designed by combination of sol–gel synthesis and selective postsynthetic modification. Mesoporous structure of synthesized materials was characterized by low-temperature nitrogen adsorption–desorption, small-angle X-ray diffraction and transmission electron microscopy. Chemical immobilization of *N*-[*N*′-(*N*′-phenyl)-2-aminophenyl]aminoalkyl groups was confirmed by IR spectral and chemical analyses of surface layer. Loading and release behaviour of synthesized drug carriers was studied in phosphate buffer solutions with pH 5.0 and pH 7.0 using doxorubicin (Dox) as a test molecule. It was found that the loading efficiency of synthesized materials determined by UV spectroscopy measurements reached 59–76%, whereas cumulative value of Dox released from silica materials equipped with molecular and supramolecular nanovalves into the phosphate buffer solution with pH 5.0 reached up to 48% and 51%, respectively. It was proved that aromatic amino groups and surface supramolecular structures localized near pore openings play an essential role in pH-controlled Dox release.

1. Introduction

Nanostructured carriers of biologically active substances have great potential for biomedical application due to the low toxicity, improved pharmacokinetics and efficacy [1–4]. However, the predominant majority of them immediately release encapsulated compounds upon dispersion in water. The preliminary drug release leads to its undesired uptake by healthy cells, substantial decrease of the amount of active substance that enters the diseased cells and reduction of the effectiveness of therapy on the whole. Therefore, controlled delivery of drugs is one of the most promising techniques for efficient treatment of diseased tissues.

MCM-41-type silicas that are capable of controlled drug release under the influence of various external stimuli are among some of the most promising materials [5–8]. This is caused by combination of unique properties of silica (high drug loading capacity, tunable pore morphology, easy functionalization, biocompatibility) with the ability of immobilized nanostructures to respond to external influences. Construction of pH-sensitive molecular [9–13] or supramolecular [14–22] pore-blocking structures on the surface of silica nanoparticles with hexagonally arranged mesoporous channels causes a great interest of scientists as a promising approach to the creation of transport systems for pH-controlled drug release. Their action is based on the difference between the acidity of the tissues in which an inflammatory process takes place and the physiological pH of healthy cells, in particular, the acidity of tumour cells is substantially lower than that of normal ones.

Despite of variety of constructed molecular or supramolecular devices preventing uncontrollable release of biologically active molecules from internal volume of MCM-41-type silica carriers, the immobilization of molecular nanovalves on silica surface with subsequent construction of supramolecular ones and comparative analysis of their action have not been carried out. The primary

THE ROYAL SOCIETY PUBLISHING

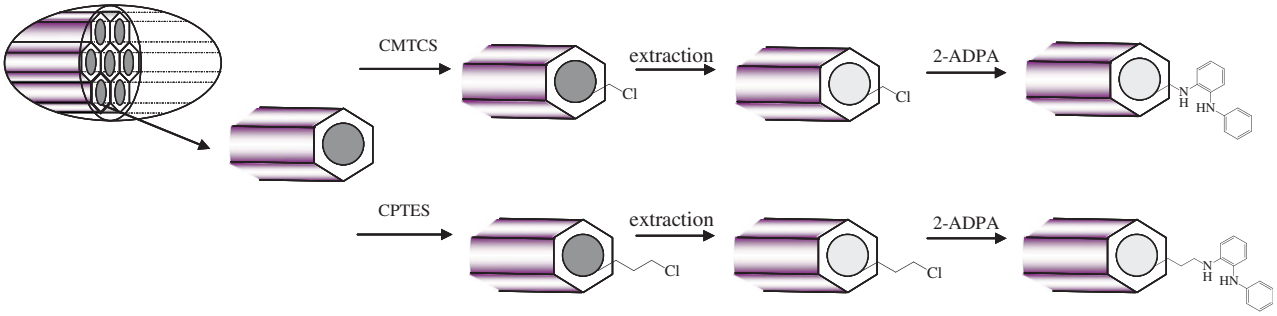

Figure 1. Schematic of selectively modified mesoporous silica nanoparticle synthesis.

objective of this work was to design silica carriers equipped with protolytically ionizable self-assembling organic moieties, molecular nanovalves, and study their effectiveness in pH-controlled delivery of biologically active substance in comparison with supramolecular ones formed with β-cyclodextrin (β-CD) participation. Doxorubicin hydrochloride (Dox), an antimitotic anthracycline antibiotic widely used in chemotherapy of solid tumours, was chosen as a model drug to assess the drug loading and releasing behaviours of synthesized silica materials. Clinical usage of Dox is limited because of its significant dose-dependent side effects which can lead to cumulative cardiotoxicity [23]. Biocompatible silica nanoparticles have been extensively studied as drug delivery systems for controlled Dox release. A variety of hollow mesoporous silica nanocages [24–29], polymer-coated [30–32] and polymer-grafted [33,34] mesoporous silica carriers, multifunctional silica nanoparticles with pH-responsive bonds [35–39], mesoporous silicas equipped with pH-sensitive nanovalves [20,40] were prepared and tested for effective delivery of Dox to tumours. In this work, pH-responsive molecular and supramolecular nanovalves were designed on the external surface of MCM-41 silica by combination of sol–gel synthesis and postsynthetic modification. The loading and release behaviour of obtained silica materials was studied to estimate their efficiency in pH-controlled Dox release.

2. Experimental

2.1. Material and methods

Tetraethyl orthosilicate TEOS (from Merck, purity ≥ 99%), (chloromethyl)trichlorosilane CMTCS (from Merck, purity ≥ 95%), (3-chloropropyl)triethoxysilane CPTES (from Aldrich, purity ≥ 95%), 2-aminodiphenylamine 2-ADPA (from Merck, purity ≥ 97%), β-CD (from Fluka, purity ≥ 99%), decyltrimethylammonium bromide DTAB (from Acros, purity ≥ 98%), acetonitrile (from Reakhim, analytical grade), Dox (from Sigma-Aldrich, purity ≥ 98%), phosphoric acid (from Reakhim, analytical grade), disubstituted sodium phosphate and monosubstituted potassium phosphate (all from Reakhim, pure analytical) were used without additional purification.

IR spectra of mesoporous silicas were recorded in frequency range from 4000 to 400 cm^{-1} using a Thermo Nicolet NEXUS FT-IR spectrophotometer.

Low-temperature nitrogen adsorption–desorption isotherms of silica materials were registered at $T = 77$ K in the region of relative pressures from 0.06 to 0.99 in increment of 0.015 with a Sorptometer Kelvin-1042. Before analysis, the silicas were degassed at 413 K under vacuum for 20 h. Specific surface area (S_{BET}) was calculated by the Brunauer–Emmett–Teller (BET) equation. The pore diameters (D) and their distributions (dV/dD) were calculated by density functional theory (DFT) method. Pore volumes were estimated at relative pressure of 0.99.

X-ray diffraction spectra were registered by use of a diffractometer DRON-4-02 with monochromatic CuK_α emission ($\lambda = 1.54178$ Å) and nickel filter. Interplanar distances (d) were estimated using Bragg diffraction equation [41]. The unit cell parameters (a) were calculated as in [42].

Transmission electron microscopy (TEM) images of initial silica were registered on a JEM-100CXII (JEOL, Japan) electron microscope at 200 kV. Silica samples were deposited onto carbon-coated copper grids as holders.

UV spectra of Dox buffer solutions were recorded at a wavelength of 483 nm with a Specord M-40. Quartz cells with 2 mm path length were used.

pH of buffer solutions were measured by an Ionometer I-160.

The content of grafted halogenoalkyl groups of mesoporous silicas was determined by the titration of chloride anions which are released as a result of alkaline hydrolysis of the C–Cl bonds [43] with mercury(II) nitrate [44]. The amount of *N*-(2-aminoethyl)-3-aminoalkyl groups of modified silicas was estimated from the results of the potentiometric titration with 0.01 M HCl. [45].

2.2. Synthesis of MCM-41-type silicas

Silica materials with hexagonally arranged uniform mesopores were synthesized using the previously reported approach [13] for base catalysed sol–gel condensation of TEOS in the presence of structure directing agent. Condensation procedure was realized in water–ethanol–ammonia solution with DTAB as a template. The molar composition of the solution was 0.1 TEOS : 0.02 DTAB : 0.47 NH_4OH : 0.47 C_2H_5OH : 13.6 H_2O. The precipitated white product was kept in the reaction mixture with stirring for 2 h, then transferred to a polypropylene bottle and aged at 373 K for 24 h. After hydrothermal treatment synthesized silica was filtered, washed with 100 ml of deionized water and dried in air at 373 K for 3 h.

Selective chemical modification of outer surface of template-containing MCM-41 silica particles with vapours of CMTCS or CPTES was carried out by use of special vacuum equipment [46]. After the chemical modification procedure the surfactant was extracted from the pore channels of CMTCS-MCM-41 and CPTES-MCM-41 silicas in acid–ethanol medium.

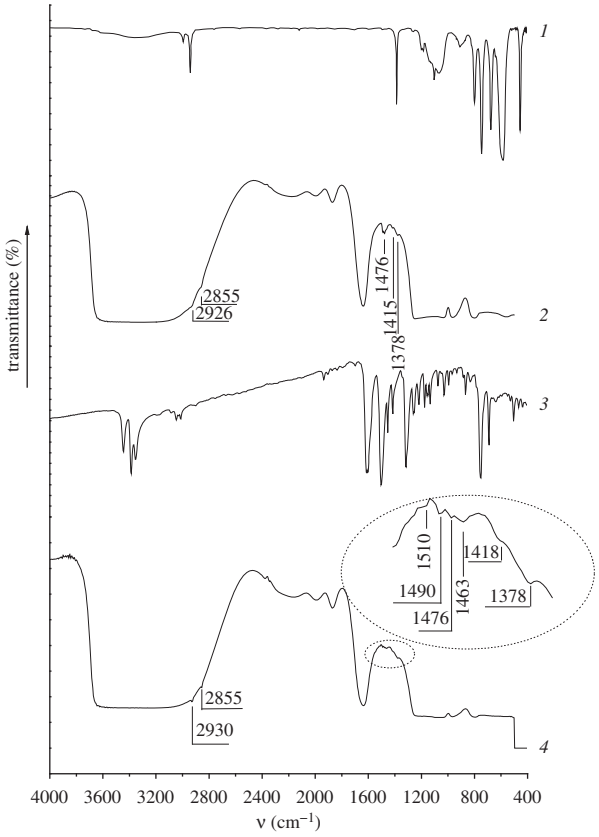

Figure 2. IR spectra of CMTCS (*1*), CMTCS-MCM-41 (*2*), ADPA (*3*) and ADPA-CMTCS-MCM-41 (*4*).

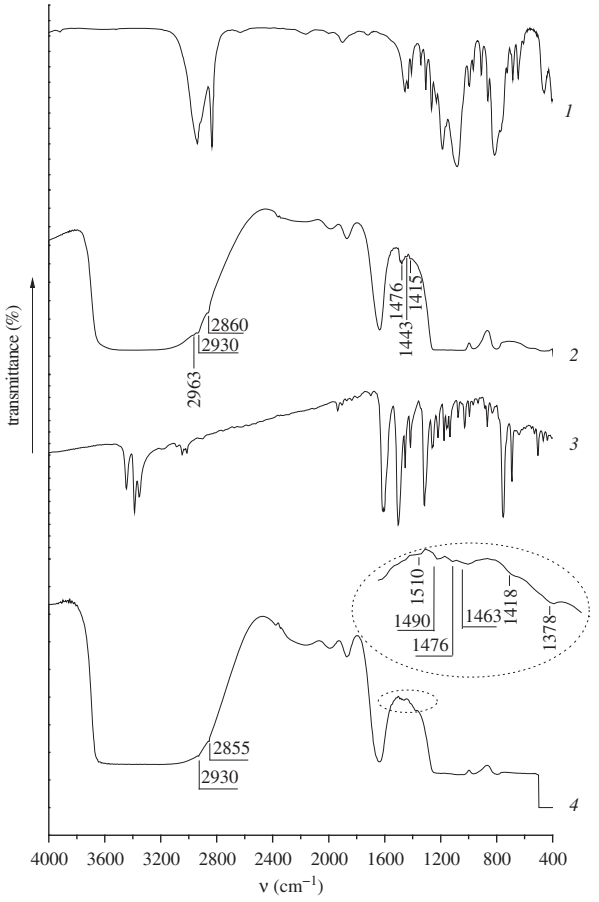

Figure 3. IR spectra of CPTES (*1*), CPTES-MCM-41 (*2*), ADPA (*3*) and ADPA-CPTES-MCM-41 (*4*).

ADPA-CMTCS-MCM-41 and ADPA-CPTES-MCM-41 silicas were prepared by reaction between primary amino groups of 2-ADPA and chloromethyl groups of CMTCS-MCM-41 or 3-chloropropyl groups of CPTES-MCM-41, correspondingly (figure 1). Briefly, halogenoalkyl silica was placed into a three-necked reactor supplied with a stirrer and a reflux condenser, and suspended in a small amount of acetonitrile at room temperature for 30 min. Then, threefold excess of 2-ADPA relative to the content of surface chloroalkyl groups was dissolved in acetonitrile and added to the reaction mixture. Modification was carried out with continuous stirring at solvent reflux temperature (355 K) for 12 h. Synthesized ADPA-CMTCS-MCM-41 and ADPA-CPTES-MCM-41 silicas were filtered and washed sequentially with acetonitrile, ethanol and distilled water. Resulting products were dried in air at 373 K for 2 h, then cooled to room temperature and kept in a desiccator before use.

2.3. Doxorubicin loading studies

Loading of Dox into the mesopore channels of silica carriers was realized in phosphate buffer solution. In particular, silica materials (0.04 g) were dispersed in Dox buffer solutions with pH = 7.0 (1 ml, 2 mg Dox ml^{-1}) and agitated at 298 K for 24 h. To construct surface nanovalves, β-CD (0.04 g) was added to the suspensions of Dox-loaded ADPA-CMTCS-MCM-41 and ADPA-CPTES-MCM-41 silicas before stirring for another 24 h. Each of the products was separated by centrifugation and rinsed with buffer solution (2 ml); the procedure was repeated twice. The supernatant solutions were collected in volumetric flasks and diluted up to 25 ml. To evaluate the content of loaded Dox its concentrations in supernatant solutions were determined by UV spectroscopy measurements at a wavelength of 483 nm.

Dox loading efficiency of silica carriers was estimated by the equation

$$\mathrm{LE} = \frac{[\mathrm{Dox}] - [\mathrm{Dox}]_S}{[\mathrm{Dox}]} \times 100\%,$$

where [Dox], the total initial content of Dox in the system (mmol g^{-1}); $[\mathrm{Dox}]_S$, content of Dox in the equilibrium supernatant buffer solution (mmol g^{-1}).

2.4. Doxorubicin release studies

To analyse the pH-controlled release, Dox-loaded silicas were redispersed in 25 ml of phosphate buffer solution with pH = 7.0 and shaken at 298 K. At certain time intervals, 2 ml of solutions were removed for analysis and replaced with a fresh portion of phosphate buffer. To generate release profile at pH = 5.0 phosphoric acid was added in the same reaction dispersion after 2 h of experiment and the liberation of Dox was studied by the previously described procedure using phosphate buffer solution with pH = 5.0. The absorbance of each collected solution was measured by UV spectroscopy at a wavelength of 483 nm and the content of released Dox was calculated taking into account the dilution of supernatant solution:

$$[\mathrm{Dox}]_R = \sum_{i=1}^{i=n} \frac{C_i \cdot V_1 - C_{i-1} \cdot V_2}{m},$$

where $[\mathrm{Dox}]_R$, content of released Dox (mmol g^{-1}); C_i, concentration measured for i portion of analysed solution

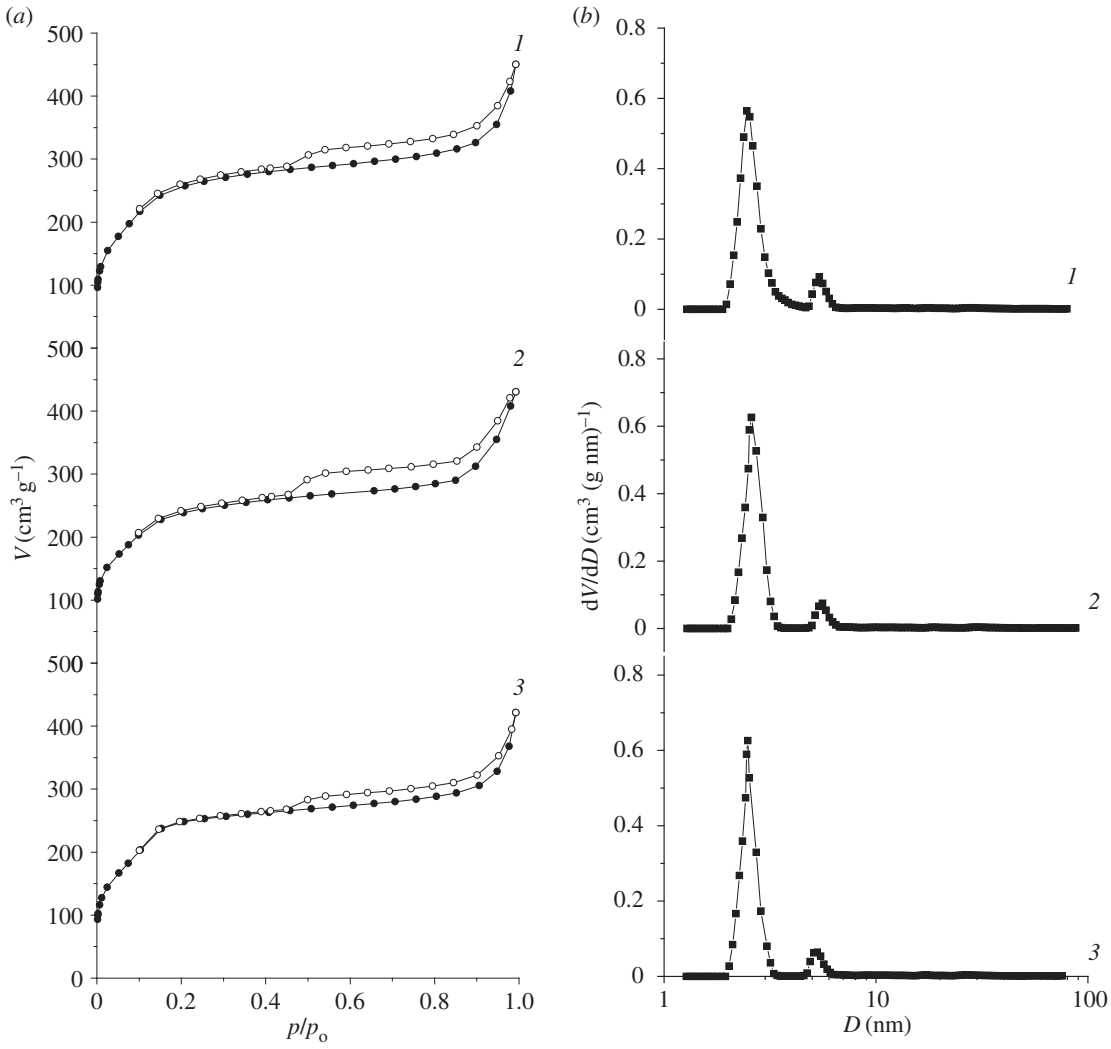

Figure 4. Nitrogen adsorption–desorption isotherms (*a*) and pore size distributions calculated by DFT method (*b*) for MCM-41 (*1*), ADPA-CMTCS-MCM-41 (*2*) and ADPA-CPTES-MCM-41 (*3*).

(mol l^{-1}); C_{i-1}, concentration measured for $i-1$ portion of analysed solution (mol l^{-1}); V_1, volume of initial solution used for Dox release studies (ml); V_2, volume of solution used for Dox release studies after aliquot removal (ml); m, the batch of Dox-loaded silica material (g).

Dox release efficiency of silica materials was calculated using

$$\mathrm{RE} = \frac{[\mathrm{Dox}]_\mathrm{R}}{[\mathrm{Dox}]_\mathrm{L}} \times 100\%,$$

where $[\mathrm{Dox}]_\mathrm{R}$, content of Dox that passes into phosphate buffer solution from the silica material (mmol g^{-1}); $[\mathrm{Dox}]_\mathrm{L}$, the initial content of Dox in the mesoporous channels of silica material (mmol g^{-1}).

3. Results and discussion

3.1. Characterization of MCM-41-type silicas

In order to prove immobilization of chloroalkyl and *N*-[*N*′-(*N*′-phenyl)-2-aminophenyl]aminoalkyl groups on silica surface, IR spectra of starting and chemically modified materials were analysed.

Introduction of chloromethyl groups in the surface layer of MCM-41 leads to the appearance of absorption bands at 2926 and 2855 cm^{-1} corresponding to the valence vibrations of the C–H bonds in methylene chains; absorption bands appear at 1476, 1415 and 1378 cm^{-1} belonging to the deformation vibrations of the C–H bonds in the CH_2 groups of grafted silane and CH_3 groups of residual template, correspondingly (figure 2, curve 2). The content of chloromethyl groups in the surface layer of synthesized CMTCS-MCM-41 determined by the titration of chloride anions which are released as a result of alkaline hydrolysis of the C–Cl bonds [43] with mercury(II) nitrate [44] equals 0.22 mmol g^{-1}.

Grafting of 3-chloropropyl groups on the surface of MCM-41 silica results in appearance of additional absorption bands in the IR spectrum of CPTES-MCM-41 (figure 3, curve 2): intense absorption bands at 2963, 2930 and 2860 cm^{-1} corresponding to the valence vibrations of the C–H bonds in 3-chloropropyl groups; absorption bands at 1476, 1443 and 1415 cm^{-1} belonging to the deformation vibrations of the C–H bonds in the CH_2 and CH_3 groups of grafted silane. The content of 3-chloropropyl groups in the surface layer of synthesized CPTES-MCM-41 is equal to 0.19 mmol g^{-1}.

After chemical immobilization of ADPA on the surface of CMTCS-MCM-41 and CPTES-MCM-41 absorption bands of the valence and deformation vibrations of the C–H bonds in the alkyl groups (2930, 2855 and 1476, 1418, 1378 cm^{-1}, correspondingly) remain in the IR spectra (figure 2, curve 4; figure 3, curve 4). Grafting of *N*-[*N*′-(*N*′-phenyl)-2-aminophenyl]aminoalkyl groups to the surface of halogenoalkyl silicas

Table 1. Structural parameters of MCM-41-type silicas.

silica	S_{BET} (m^2g^{-1})	V (cm^3g^{-1})	D_{DFT} (nm)	d_{100} (nm)	a (nm)
MCM-41	1003	0.69	2.42, 5.29	3.07	3.54
ADPA-CMTCS-MCM-41	840	0.66	2.50, 5.29	3.07	3.54
ADPA-CPTES-MCM-41	780	0.65	2.48, 5.29	3.09	3.56

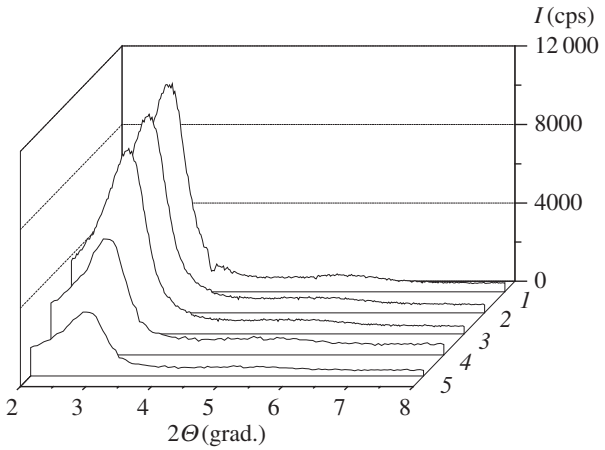

Figure 5. X-ray diffraction patterns of MCM-41 (*1*), CMTCS-MCM-41 (*2*), CPTES-MCM-41 (*3*), ADPA-CMTCS-MCM-41 (*4*) and ADPA-CPTES-MCM-41 (*5*).

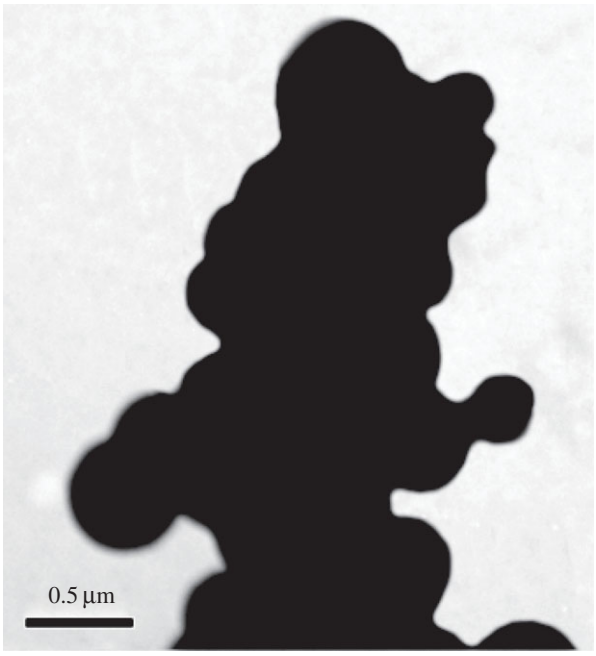

Figure 6. TEM image of parent MCM-41.

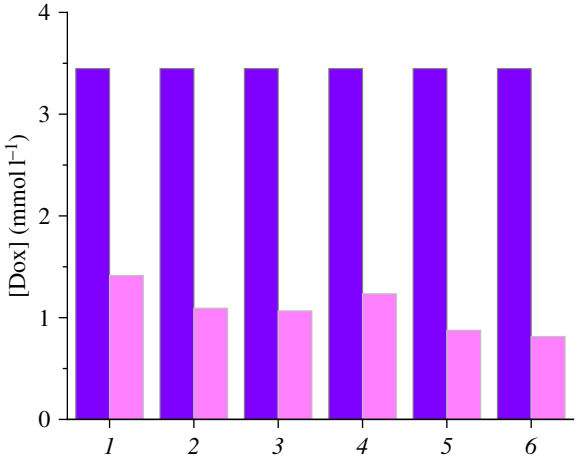

Figure 7. Changes of Dox concentration from initial (dark colour) to equilibrium (light colour) values after contact with CMTCS-MCM-41 (*1*), ADPA-CMTCS-MCM-41 (*2*), β-CD-ADPA-CMTCS-MCM-41 (*3*), CPTES-MCM-41 (*4*), ADPA-CPTES-MCM-41 (*5*) and β-CD-ADPA-CPTES-MCM-41 (*6*).

leads to the appearance of characteristic absorption bands in the range of 1450–1550 cm^{-1}, which belong to the valence vibrations of the C=C bonds in the aromatic groups (figures 2 and 3). Moreover, the intensity of the absorption band at 1378 cm^{-1} corresponding to the deformation vibrations of the C–H bonds in the CH_2 groups increases substantially due to the additional contribution of the valence vibrations of the C–N bonds in the secondary amino groups. Characteristic absorption bands of the valence and deformation vibrations of the N–H bonds in the grafted aromatic amino groups are not registered in the IR spectra of CMTCS-MCM-41 and CPTES-MCM-41 because they overlap with the absorption bands of the valence vibrations of the O–H bonds in the surface silanol groups, and also with the valence and deformation vibrations of the O–H bonds in the adsorbed water molecules. The content of *N*-[*N*′-(*N*′-phenyl)-2-aminophenyl]aminomethyl and *N*-[*N*′-(*N*′-phenyl)-2-aminophenyl]-3-aminopropyl groups in ADPA-CMTCS-MCM-41 and ADPA-CPTES-MCM-41 silicas estimated from the results of the potentiometric titration with 0.01 M HCl [45] is equal to 0.15 mmol g^{-1}.

Low-temperature nitrogen adsorption–desorption isotherms of MCM-41, ADPA-CMTCS-MCM-41 and ADPA-CPTES-MCM-41 (figure 4) were used to evaluate structural parameters of synthesized silica materials (table 1). S_{BET} was calculated according to the multi-point BET method [47]. The pore diameters (D) and their distributions (dV/dD) were determined in accordance with the DFT method [48–50]. The total pore volume (V) was estimated from the amount of adsorbed nitrogen at a relative pressure of 0.99.

Represented isotherms reveal the II-type in BET classification [47] and exhibit a sharp increase at relative pressures up to 0.2, which is associated with monolayer formation. Capillary condensation of nitrogen in the mesopore channels of silica materials with a narrow pore size distribution takes place at higher relative pressures (figure 4). The analysis of structural parameters demonstrates decrease in the specific surface area caused by chemical bonding of *N*-[*N*′-(*N*′-phenyl)-2-aminophenyl]aminomethyl (or N-[N′-(N′-phenyl)-2-aminophenyl]-3-aminopropyl) groups in surface layer of parent MCM-41 (table 1). However, no substantial changes are observed in values of pore diameter and total pore volume after chemical modification of MCM-41. This can be explained by

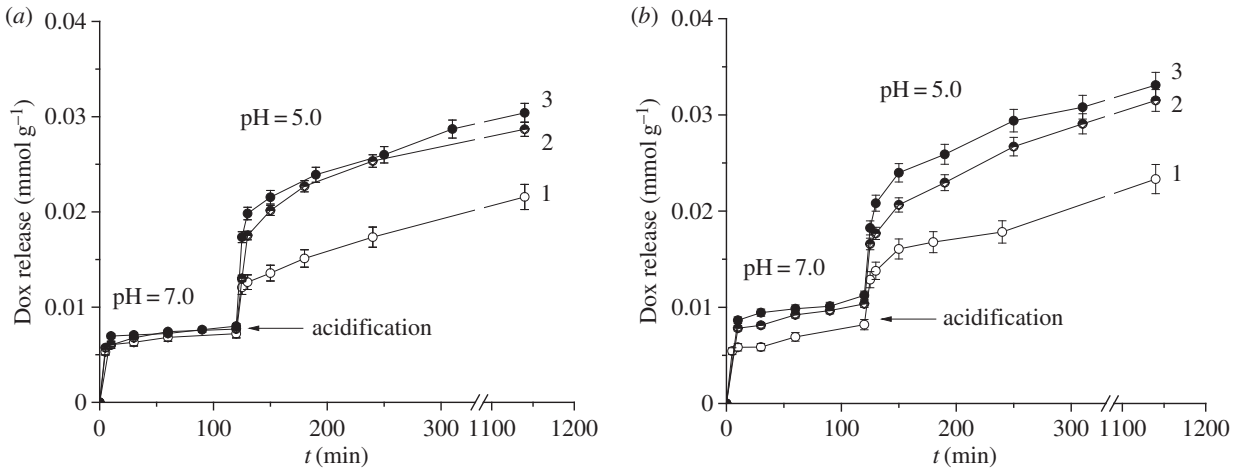

Figure 8. pH-dependent cumulative doxorubicin release: (*a*) from CMTCS-MCM-41 (1), ADPA-CMTCS-MCM-41 (2), β-CD-ADPA-CMTCS-MCM-41 (3); (*b*) from CPTES-MCM-41 (1), ADPA-CPTES-MCM-41 (2), β-CD-ADPA-CPTES-MCM-41 (3).

Table 2. The efficiency of Dox loading and release by MCM-41-type silica carriers.

silica	loading efficiency (%)	release efficiency at pH = 7.0 (%)	release efficiency at pH = 5.0 (%)
CMTCS-MCM-41	59	14.18	42.41
ADPA-CMTCS-MCM-41	68	13.08	48.70
β-CD-ADPA-CMTCS-MCM-41	69	13.44	51.07
CPTES-MCM-41	64	14.63	42.14
ADPA-CPTES-MCM-41	75	16.11	48.97
β-CD-ADPA-CPTES-MCM-41	76	17.07	50.28

immobilization of organic groups exceptionally on the external surface of silica materials.

To confirm hexagonally ordered pore structure and obtain information about interplanar distances and unit cell parameters of synthesized silicas, small-angle X-ray diffraction was applied. Silica materials of MCM-41 type are characterized by the presence of from one to five reflections in the small-angle region (2θ from 2° to 7°) [51]. Decreasing of template hydrocarbon chain length or variation of the synthesis conditions often leads to the reduction of quantity of reflections in the diffractograms [52]. As can be seen in figure 5, intense reflection of interference index (100) is registered on the X-ray diffraction patterns of parent MCM-41 and CMTCS-MCM-41, CPTES-MCM-41, ADPA-CMTCS-MCM-41, ADPA-CPTES-MCM-41 silicas, indicating the presence of recurring structural units (in this case the pores with a narrow size distribution) in the synthesized materials. Position of diffraction peak corresponding to (100) reflection of silicas with chemically immobilized chloroalkyl groups (figure 5) is in a good agreement with its location for parent MCM-41 silica ($2\theta = 2.88°$). So, vapour-phase treatment of template-containing MCM-41 with chloroalkylsilanes has no substantial effect on its structure. Chemical immobilization of *N*-[*N*′-(*N*′-phenyl)-2-aminophenyl]aminoalkyl groups on CMTCS-MCM-41 and CPTES-MCM-41 particles also does not lead to a notable change in the low-angle peak position (figure 5). Obtained results confirm modification of only outer surface of chloroalkyl silicas and preservation of their structural parameters after postsynthetic activation with 2-ADPA (table 1). At the same time, broadening of (100) reflection and lowering of its intensity for ADPA-CMTCS-MCM-41 and ADPA-CPTES-MCM-41 compared with parent

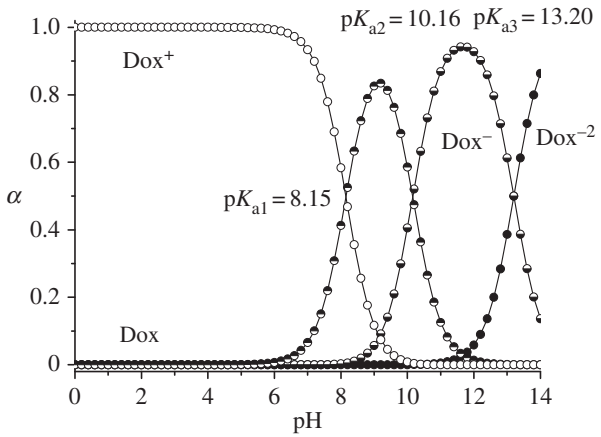

Figure 9. Distribution curves of doxorubicin protolytic forms.

MCM-41 implies some long-range distortion of the hexagonal arrangement of mesopore channels (figure 5).

As can be seen from the TEM images, nanoparticles of MCM-41 silica are spherically shaped (figure 6). Their mean diameter is about 0.4 μm.

3.2. Doxorubicin loading and release

Loading of mesoporous channels of silica carriers with Dox molecules was realized from phosphate buffer solution with drug content near that necessary for monolayer formation. As can be seen from figure 7, concentration of Dox in supernatant solution decreases substantially after the interaction with MCM-41-type silicas. The loading efficiency of synthesized materials determined by UV

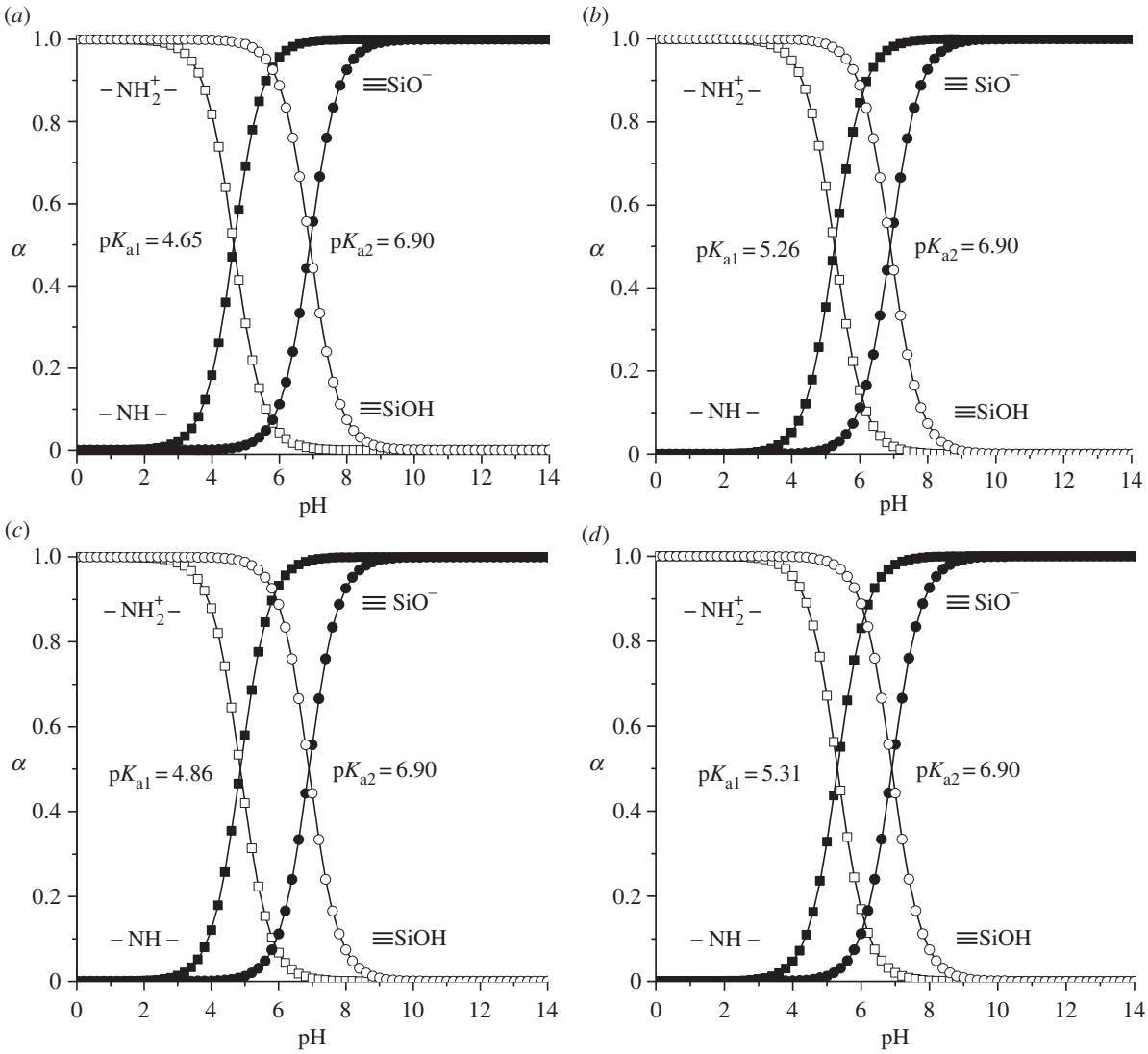

Figure 10. Distribution curves of protolytic forms of surface silanol and secondary amino groups of ADPA-CMTCS-MCM-41 (*a*), β-CD-ADPA-CMTCS-MCM-41 (*b*), ADPA-CPTES-MCM-41 (*c*) and β-CD-ADPA-CPTES-MCM-41 (*d*) silicas.

spectroscopy measurements reaches 59–76% (table 2). It was found that despite the lack of *N*-[*N*′-(*N*′-phenyl)-2-aminophenyl]aminoalkyl group contribution to adsorption of Dox on ADPA-CMTCS-MCM-41 and ADPA-CPTES-MCM-41 silicas, the loading of drug into amino-containing silicas is slightly higher compared with chloroalkyl ones. Obviously, aromatic amino groups that were immobilized on the external surface of silica particles protect adsorbed drug molecules from elution by rinsing with small amounts of buffer solution with pH = 7.0 and enhance Dox retention in the mesopores, and, as a result, cause an increase in loading capacity on the whole. A similar pattern is observed for silica carriers equipped with supramolecular nanovalves (figure 7; table 2).

The creation of efficient drug delivery system along with the high loading capacity and the ability of silica carrier to store and release biologically active substances on demand has substantial importance. In order to prove that the drug liberation can be controlled by pH-responsive molecular and supramolecular nanovalves, the release of Dox from silicas with chemically immobilized chloroalkyl and *N*-[*N*′-(*N*′-phenyl)-2-aminophenyl]aminoalkyl groups as well as equipped with macrocyclic oligosaccharide component was studied. Obtained results are summarized in figure 8 and table 2. It can be seen that Dox liberation is both time- and pH-dependent (figure 8). Rapid delivery of Dox at pH = 7.0 occurs only within the first ten minutes. Obviously, transition of drug molecules localized on the external surface of silica particles and nearby pore openings into the phosphate buffer medium takes place in this time interval. Then Dox release rate decreases significantly due to the delivery of molecules that are located inside carrier mesopores. As seen from figure 8, the leakage of Dox from silica carriers at pH = 7.0 is negligible in time interval from 10 to 120 min. It can be supposed that this process is limited not only by the diffusion through the mesopore channels but also by hydrogen bond formation and electrostatic interactions between Dox molecules and surface of organosilicas. The retention of Dox at pH = 7.0 can be clearly explained on the basis of analysis of protolytic properties of Dox and functional groups of organosilicas (figures 9 and 10). Thus, in the phosphate buffer solution with pH = 7.0 approximately 56% of the silanol groups located in pores of organosilicas are ionized, whereas 93% of Dox daunosamine groups are protonated. Negatively charged Si−O$^-$ groups are able to interact electrostatically with the positively charged protonated primary amino groups of Dox. Moreover, residual unprotonated daunosamine groups can form hydrogen bonds with silanol groups of MCM-41. At the same time, *N*-[*N*′-(*N*′-phenyl)-2-aminophenyl]aminoalkyl groups, immobilized on the

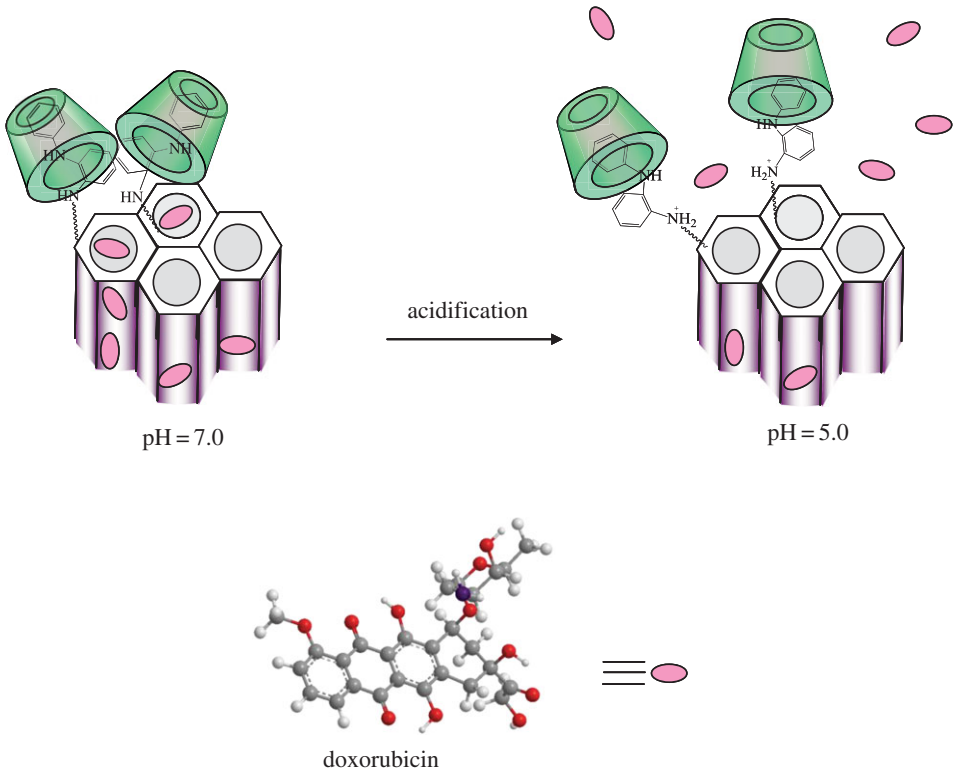

Figure 11. pH-controlled liberation of doxorubicin by silica carriers equipped with supramolecular nanovalves.

external surface of silica particles, do not contribute to the adsorption process because at pH = 7.0 their secondary amino groups are protonated (positively charged) (figure 10).

Despite small Dox quantities liberated from the mesoporous channels of silica carriers during kinetic experiments at pH = 7.0, the drug quickly passes into solution on pH lowering (figure 8). It can be supposed that aromatic amino groups cooperate at pH = 7.0 and serve as molecular nanovalves preventing Dox release from mesopore channels [13]. Decrease of pH leads to the protonation of the secondary amino groups of surface organic radicals, their repulsion, and subsequent opening of pore orifices. Similar behaviour is observed for silica carriers equipped with supramolecular nanovalves: protonation of aromatic amino groups leads to their repulsion and simultaneous decrease of surface inclusion complex stability that is accompanied with drifting of oligosaccharide moieties further from the silica surface (figure 11). Moreover, on acidifying of suspension to pH = 5.0 non-ionized surface silanol groups lose their ability to interact with protonated amino groups of Dox (figures 9 and 10). The pH-dependent Dox release behaviour increases in the series CMTCS-MCM-41 < ADPA-CMTCS-MCM-41 < β-CD-ADPA-CMTCS-MCM-41 and CPTES-MCM-41 < ADPA-CPTES-MCM-41 < β-CD-ADPA-CPTES-MCM-41 confirming the essential role of chemically immobilized aromatic amino groups and surface supramolecular structures in the controlled delivery of biologically active substance on pH change. The most pronounced pH-controlled effect on Dox liberation is observed for silica carriers that are equipped with supramolecular nanostructures localized near pore orifices. Obviously, bulky β-CD macromolecules of surface supramolecular complex block pore entrances more effectively than aromatic amino groups. They provide higher loading as well as release efficiency of silica carriers. The cumulative value of Dox released from β-CD-ADPA-CMTCS-MCM-41 and β-CD-ADPA-CPTES-MCM-41 silicas into the phosphate buffer solution with pH = 5 reached up to 50% after contact for 17 h (table 2).

4. Conclusion

In this work, silica carriers equipped with pH-responsive molecular or supramolecular nanovalves were designed for controlled delivery of drug (Dox) molecules. Chemical immobilization of aromatic amine radicals on the surface of mesoporous silica was realized by combination of sol–gel synthesis and selective postsynthetic modification of external surface by assembly method. It was proved that supramolecular nanovalves that are formed by surface aromatic amino groups and β-CD macromolecules supplied from solution block the mesopore openings in neutral medium more efficiently than molecular ones. Liberation of Dox takes place under mildly acidic conditions. The stability of inclusion complexes formed between cyclic oligosaccharide (β-CD) and surface *N*-[*N*′-(*N*′-phenyl)-2-aminophenyl]aminoalkyl radicals decreases substantially on protonation of their secondary amino groups. So, β-CD moieties drift further from the surface, whereas positively charged amino groups repulse each other, providing unhindered Dox liberation.

Authors' contributions. N.V.R. planned experimental work, realized sol–gel synthesis and selective postsynthetic modification of silica surface, carried out drug loading and release studies, participated in data analysis, drafted the manuscript. L.A.B. supervised the work, participated in results interpretation and writing of the manuscript. All authors gave final approval for publication.

Competing interests. We declare we have no competing interests.

Funding. We received no funding for this study.

References

1. Murthy SK. 2007 Nanoparticles in modern medicine: state of the art and future challenges. *Int. J. Nanomed*. **2**, 129–141.
2. Brigger I, Dubernet C, Couvreur P. 2012 Nanoparticles in cancer therapy and diagnosis. *Adv. Drug Del. Rev*. **64**, 24–36. (doi:10.1016/j.addr.2012.09.006)
3. Yang P, Gai S, Lin J. 2012 Functionalized mesoporous silica materials for controlled drug delivery. *Chem. Soc. Rev*. **41**, 3679–3698. (doi:10.1039/C2CS15308D)
4. Mamaeva V, Sahlgren C, Linden M. 2013 Mesoporous silica nanoparticles in medicine—recent advances. *Adv. Drug Del. Rev*. **65**, 689–702. (doi:10.1016/j.addr.2012.07.018)
5. Li Z, Barnes JC, Bosoy A, Stoddart JF, Zink JI. 2012 Mesoporous silica nanoparticles in biomedical applications. *Chem. Soc. Rev*. **41**, 2590–2605. (doi:10.1039/C1CS15246G)
6. Slowing II, Vivero-Escoto JL, Wu C-W, Lin VS-Y. 2008 Mesoporous silica nanoparticles as controlled release drug delivery and gene transfection carriers. *Adv. Drug Del. Rev*. **60**, 1278–1288. (doi:10.1016/j.addr.2008.03.012)
7. Zhu C-L, Wang X-W, Lin Z-Z, Xie Z-H, Wang X-R. 2014 Cell microenvironment stimuli-responsive controlled-release delivery systems based on mesoporous silica nanoparticles. *J. Food Drug Anal*. **22**, 18–28. (doi:10.1016/j.jfda.2014.01.002)
8. Chen T, Yang N, Fu J. 2013 Controlled release of cargo molecules from hollow mesoporous silica nanoparticles based on acid and base dual-responsive cucurbit[7]uril pseudorotaxanes. *Chem. Commun*. **49**, 6555–6557. (doi:10.1039/c3cc43221a)
9. Gan Q, Lu X, Dong W, Yuan Y, Qian J, Li Y, Shi J, Liu C. 2012 Endosomal pH-activatable magnetic nanoparticle-capped mesoporous silica for intracellular controlled release. *J. Mater. Chem*. **22**, 15 960–15 968. (doi:10.1039/C2JM32020G)
10. Casasus R *et al.* 2004 Toward the development of ionically controlled nanoscopic molecular gates. *J. Am. Chem. Soc*. **126**, 8612–8613. (doi:10.1021/ja048095i)
11. Casasus R, Climent E, Marcos MD, Martinez-Manez R, Sansenon F, Soto J, Amoros P, Cano J, Ruiz E. 2008 Dual aperture control on pH- and anion-driven supramolecular nanoscopic hybrid gate-like ensembles. *J. Am. Chem. Soc*. **130**, 1903–1917. (doi:10.1021/ja0756772)
12. Bernardos A, Aznar E, Coll C, Martinez-Manez R, Barat JM, Marcos MD, Sancenon F, Benito A, Soto J. 2008 Controlled release of vitamin B2 using mesoporous materials functionalized with amine-bearing gate-like scaffoldings. *J. Control. Release* **131**, 181–189. (doi:10.1016/j.jconrel.2008.07.037)
13. Roik NV, Belyakova LA. 2014 Chemical design of pH-sensitive nanovalves on outer surface of mesoporous silicas for controlled storage and release of aromatic amino acid. *J. Solid State Chem*. **215**, 284–291. (doi:10.1016/j.jssc.2014.04.018)
14. Gao Y, Yang C, Liu X, Ma R, Kong D, Shi L. 2012 A multifunctional nanocarrier based on nanogated mesoporous silica for enhanced tumor-specific uptake and intracellular delivery. *Macromol. Biosci*. **12**, 251–259. (doi:10.1002/mabi.201100208)
15. Yang Y-W. 2011 Towards biocompatible nanovalves based on mesoporous silica nanoparticles. *Med. Chem. Commun*. **2**, 1033–1049. (doi:10.1039/C1MD00158B)
16. Ambrogio MW, Thomas CR, Zhao Y-L, Zink JI, Stoddart JF. 2011 Mechanized silica nanoparticles: a new frontier in theranostic nanomedicine. *Acc. Chem. Res*. **44**, 903–913. (doi:10.1021/ar200018x)
17. Nguyen TD, Leung KC-F, Liong M, Pentecost CD, Stoddart JF, Zink JI. 2006 Construction of a pH-driven supramolecular nanovalve. *Org. Lett*. **8**, 3363–3366. (doi:10.1021/ol0612509)
18. Klichko Y, Khashab NM, Yang Y-W, Angelos S, Stoddart JF, Zink JI. 2010 Improving pore exposure in mesoporous silica films for mechanized control of the pores. *Microporus Mesoporus Mater*. **132**, 435–441. (doi:10.1016/j.micromeso.2010.03.024)
19. Angelos S, Yang Y-W, Patel K, Stoddart JF, Zink JI. 2008 pH-Responsive supramolecular nanovalves based on cucurbit[6]uril pseudorotaxanes. *Angew. Chem. Int. Ed*. **120**, 2254–2258. (doi:10.1002/ange.200705211)
20. Meng H, Xue M, Xia T, Zhao Y-L, Tamanoi F, Stoddart JF, Zink JI, Nel AE. 2010 Autonomous *in vitro* anticancer drug release from mesoporous silica nanoparticles by pH-sensitive nanovalves. *J. Am. Chem. Soc*. **132**, 12 690–12 697. (doi:10.1021/ja104501a)
21. Park C, Oh K, Lee SC, Kim C. 2007 Controlled release of guest molecules from mesoporous silica particles based on a pH-responsive polypseudorotaxane motif. *Angew. Chem. Int. Ed*. **46**, 1455–1457. (doi:10.1002/anie.200603404)
22. Wang T, Wang MD, Ding CD, Fu JJ. 2014 Mono-benzimidazole functionalized β-cyclodextrins as supramolecular nanovalves for pH-triggered release of *p*-coumaric acid. *Chem. Commun*. **50**, 12 469–12 472. (doi:10.1039/c4cc05677a)
23. Sumeet G, Swati M. 2014 *Doxorubicin induced cardiotoxicity: the spice retreat*. Saarbruecken, Germany: Lambert Academic Publishing.
24. Gao Y, Chen Y, Ji X, He X, Yin Q, Zhang Z, Shi J, Li Y. 2011 Controlled intracellular release of doxorubicin in multidrug-resistant cancer cells by tuning the shell-pore sizes of mesoporous silica nanoparticles. *Am. Chem. Sci*. **5**, 9788–9798. (doi:10.1021/nn2033105)
25. Tan S, Wu Q, Wang J, Wang Y, Liu X, Sui K, Deng X, Wang H, Wu M. 2011 Dynamic self-assembly synthesis and controlled release as drug vehicles of porous hollow silica nanoparticles. *Microporus Mesoporus Mater*. **142**, 601–608. (doi:10.1016/j.micromeso.2011.01.004)
26. Wang T *et al.* 2011 Uniform hollow mesoporous silica nanocages for drug delivery *in vitro* and *in vivo* for liver cancer therapy. *Mater. Chem*. **21**, 5299–5306. (doi:10.1039/C0JM04115G)
27. Mishra AK, Pandey H, Agarwal V, Ramteke PW, Pandey AC. 2014 Nanoengineered mesoporous silica nanoparticles for smart delivery of doxorubicin. *J. Nanoparticle Res*. **16**, 2515. (doi:10.1007/s11051-014-2515-y)
28. Yang J, Lee J, Kang J, Lee K, Suh J-S, Yoon H-G, Huh Y-M, Haam S. 2008 Hollow silica nanocontainers as drug delivery vehicles. *Langmuir* **24**, 3417–3421. (doi:10.1021/la701688t)
29. Knezevic NZ, Ruiz-Hernandez E, Hennink WE, Vallet-Regi M. 2013 Magnetic mesoporous silica-based core/shell nanoparticles for biomedical applications. *RSC Adv*. **3**, 9584–9593. (doi:10.1039/C3RA23127E)
30. Hu X, Hao X, Wu Y, Zhang J, Zhang X, Wang PC, Zou G, Liang X-J. 2013 Multifunctional hybrid silica nanoparticles for controlled doxorubicin loading and release with thermal and pH dual response. *J. Mater. Chem. B* **1**, 1109–1118. (doi:10.1039/C2TB00223J)
31. Chen Y, Yang W, Chang B, Hu H, Fang X, Sha X. 2013 *In vivo* distribution and antitumor activity of doxorubicin-loaded N-isopropylacrylamide-co-methacrylic acid coated mesoporous silica nanoparticles and safety evaluation. *Eur. J. Pharm. Biopharm*. **85**, 406–412. (doi:10.1016/j.ejpb.2013.06.015)
32. Singh N, Karambelkar A, Gu L, Lin K, Miller JS, Chen CS, Sailor MJ, Bhatia SN. 2011 Bioresponsive mesoporous silica nanoparticles for triggered drug release. *J. Am. Chem. Soc*. **133**, 19 582–19 585. (doi:10.1021/ja206998x)
33. Yuan L, Tang Q, Yang D, Zhang JZ, Zhang F, Hu J. 2011 Preparation of pH-responsive mesoporous silica nanoparticles and their application in controlled drug delivery. *J. Phys. Chem. C* **115**, 9926–9932. (doi:10.1021/jp201053d)
34. Gu J, Su S, Zhu M, Li Y, Zhao W, Duan Y, Shi J. 2012 Targeted doxorubicin delivery to liver cancer cells by PEGylated mesoporous silica nanoparticles with a pH-dependent release profile. *Microporus Mesoporus Mater*. **161**, 160–167. (doi:10.1016/j.micromeso.2012.05.035)
35. Lee JE, Lee DJ, Lee N, Kim BH, Choi SH, Hyeon T. 2011 Multifunctional mesoporous silica nanocomposite nanoparticles for pH controlled drug release and dual modal imaging. *J. Mater. Chem*. **21**, 16 869–16 872. (doi:10.1039/C1JM11869B)
36. Knezevic NZ, Trewyn BG, Lin VS-Y. 2011 Light- and pH-responsive release of doxorubicin from a mesoporous silica-based nanocarrier. *Chem. Eur. J*. **17**, 3338–3342. (doi:10.1002/chem.201002960)
37. Lee C-H, Cheng S-H, Huang I-P, Souris JS, Yang C-S, Mou C-Y, Lo L-W. 2010 Intracellular pH-responsive mesoporous silica nanoparticles for the controlled release of anticancer chemotherapeutics. *Angew.*

Chem. **122**, 8390–8395. (doi:10.1002/ange.201002639)

38. Zhang X, Clime L, Roberge H, Normandin F, Yahia LH, Sacher E, Veres T. 2011 pH-Triggered doxorubicin delivery based on hollow nanoporous silica nanoparticles with free-standing superparamagnetic Fe_3O_4 cores. *J. Phys. Chem. C* **115**, 1436–1443. (doi:10.1021/jp1075498)
39. Wang T, Sun G, Wang M, Zhou B, Fu JJ. 2015 Voltage/pH driven mechanized silica nanoparticles for the multimodal controlled release of drugs. *ACS Appl. Mater. Interfaces* **7**, 21 295–21 304. (doi:10.1021/acsami.5b05619)
40. Ding CD, Liu Y, Wang T, Fu J. 2016 Triple-stimuli-responsive nanocontainers assembled by water-soluble pillar[5]arene-based pseudorotaxanes for controlled release. *J. Mater. Chem. B* **4**, 2819–2827. (doi:10.1039/C6TB00459H)
41. Bragg WL. 1913 The diffraction of short electromagnetic waves by a crystal. *Proc. Camb. Philos. Soc.* **17**, 43–57.
42. Fenelonov VB, Romannikov VN, Derevyankin AYu. 1999 Mesopore size and surface area calculations for hexagonal mesophases (types MCM-41, FSM-16, etc.) using low-angle XRD and adsorption data. *Microporus Mesoporus Mater*. **28**, 57–72. (doi:10.1016/S1387-1811(98)00280-7)
43. Pohloudek-Fabini R, Beyrich Th. 1975 *Organische analyse*. Leipzig, Germany: Akademische Verlagsgesellschart Geest und Portig K.-G.
44. Williams WJ. 1979 *Handbook of anion determination*. London, UK: Butterworths.
45. Helfferich FG. 1995 *Ion exchange*. New York, NY: Dover Publications Inc.
46. Roik NV, Belyakova LA. 2013 Sol-gel synthesis of MCM-41 silicas and selective vapor-phase modification of their surface. *J. Solid State Chem*. **207**, 194–202. (doi:10.1016/j.jssc.2013.09.027)
47. Brunauer S, Emmet PH, Teller E. 1938 Adsorption of gases in multimolecular layers. *J. Am. Chem. Soc.* **60**, 309–319. (doi:10.1021/ja01269a023)
48. Thommes M. 2010 Physical adsorption characterization of nanoporous materials. *Chem. Ing. Tech*. **82**, 1059–1073. (doi:10.1002/cite.201000064)
49. Evans R, Marconi UMB, Tarazona P. 1986 Capillary condensation and adsorption in cylindrical and slit-like pores. *J. Chem. Soc. Faraday Trans. 2* **82**, 1763–1787. (doi:10.1039/F29868201763)
50. Neimark AV, Ravikovitch PI, Grün M, Schüth F, Unger KK. 1998 Pore size analysis of MCM-41 type adsorbents by means of nitrogen and argon adsorption. *J. Coll. Int. Sci*. **207**, 159–169. (doi:10.1006/jcis.1998.5748)
51. Kruk M, Jaroniec M. 1999 Characterization of highly ordered MCM-41 silicas using X-ray diffraction and nitrogen adsorption. *Langmuir* **15**, 5279–5284. (doi:10.1021/la990179v)
52. Sayari A, Yang Y. 2000 Highly ordered MCM-41 silica prepared in the presence of decyltrimethylammonium bromide. *J. Phys. Chem. B* **104**, 4835–4839. (doi:10.1021/jp0001900)